The Principles of α-Helix Formation: Explaining Complex Kinetics with Nucleation−Elongation Theory

Urmi R. Doshi[†] and Victor Muñoz*

Department of Chemistry and Biochemistry and Center for Biomolecular Structure and Organization, University of Maryland, College Park, Maryland 20742

Received: January 8, 2004; In Final Form: March 17, 2004

Helix−coil theory has proven to be extremely successful in describing the stability of α-helices. However, less is known about the applicability of the nucleation−elongation model to the kinetics of α-helix formation. A recent nanosecond infrared temperature-jump study in a helix-forming peptide has revealed unprecedented kinetic complexity (Huang, C. Y.; Getahun, Z.; Zhu, Y. J.; Klemke, J. W.; DeGrado, W. F.; Gai, F. *Proc. Natl. Acad. Sci. U.S.A.* **2002**, *99*, 2788−2793). In this investigation, the apparent kinetic relaxation varies depending on the location of the spectroscopic probe on the molecule and on the magnitude of the perturbation (*T*-jump size). In an effort to rationalize these results, we have developed a detailed kinetic model of α-helix formation. The model is based on a simple nucleation−elongation description of α-helix formation and incorporates sequence dependence factors from a previous equilibrium implementation of helix−coil theory (AGADIR; Muñoz, V.; Serrano, L. *Nat. Struct. Biol.* **1994**, *1*, 399−409). Combining the model and an elementary description of the peptide bond amide I spectrum, we successfully simulate the experiments of Huang et al. Analysis of the simulations reveals that the dependence of the kinetic relaxation on the location of the spectroscopic probe is a consequence of helix fraying at the ends. End fraying is a general property of the helix−coil transition, which, in this case, is further modulated by strong capping effects. The decrease in apparent relaxation time the larger the perturbation is also an indirect consequence of different distributions of helical lengths at each initial condition. Our results demonstrate that nucleation−elongation is a valid mechanistic description of the kinetic process of α-helix formation. Furthermore, from the comparison between the experiments of Huang et al. and our calculations we can conclude that the cost in nucleating a helix is small and that the 150−300 ns relaxation observed in many *T*-jump experiments corresponds, indeed, to reequilibration between the coil and helix ensembles. The success of our kinetic model of α-helix formation opens the possibility of making specific predictions that can be tested experimentally.

Introduction

The principles governing the formation of α-helices have been the subject of intensive investigation for the last 5 decades. From a structural standpoint, the α-helix is one of the most abundant and important motifs found in natural proteins. The helix−coil transition is also a paradigmatic example of the complex conformational transitions expected to occur in polymers. It is for these reasons that theoretical models describing the thermodynamic properties of the helix−coil transition were already formulated in the late 1950s and early 1960s.[3,4] In these theoretical treatments, α-helix formation is described as a simple nucleation−elongation process. Nucleation is always unfavorable, but it can occur at any position of the molecule. Elongating from the helix nucleus is fundamentally isoenergetic with different amino acid sequences having small favorable or unfavorable biases. Because the nucleation cost in natural sequences seems to be only a few kilocalories per mole,[5] helix−coil theory predicts that α-helix formation is a complex process that deviates greatly from an all or none transition. The most relevant predictions of equilibrium helix−coil theory have successfully withstood detailed experimental scrutiny. The expected stabilization of the α-helix conformation as the length of the polymer increases was dramatically demonstrated using peptides with varying numbers of a basic repeating unit.[6−8] The helix fraying at the ends of the molecule has also been observed directly in hydrogen−deuterium exchange experiments,[9,10] and indirectly monitoring the perturbation in helix stability induced by incorporating helix breaker residues in different positions of host helical peptides.[11−15] Guest−host experiments have also been extremely useful in measuring the role of many energetic factors involved in the stabilization of α-helices, such as capping effects, $i, i+3$ and $i, i+4$ side chain−side chain interactions, and helix macrodipole effects.[5,16] All of this work crystallized in the formulation of helix−coil models capable of predicting the helix propensity of any given amino acidic sequence with remarkable precision.[2]

The kinetics of α-helix formation has been a more recent subject of experimental study. After the pioneering work of Schwarz and collaborators on very long homopolymers,[17] it was the development of laser-induced temperature-jump (*T*-jump) instrumentation that permitted the experimental investigation of the helix−coil kinetics in protein-like α-helices.[18] *T*-jump experiments have clearly shown that short polyalanine α-helices form in ∼200 ns at room temperature, but the relaxation times observed with different spectroscopical probes differ slightly.[18−21] Such results have been successfully described with a detailed nucleation−elongation kinetic model,[21] which predicts that

* To whom correspondence should be addressed. Phone: 1-301-405-3165. Fax: 1-301-314-0386. E-mail: vm48@umail.umd.edu.
† E-mail: urdoshi@wam.umd.edu.

10.1021/jp049896a CCC: $27.50
Published on Web 05/20/2004

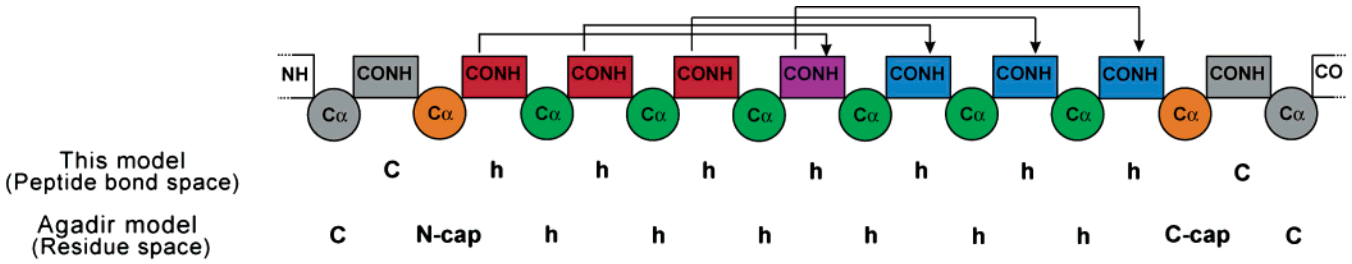

Figure 1. Model of α-helix formation. The figure displays a segment of α-helix structure together with conformational assignments based on residues (AGADIR) and based on peptide bonds (this work). Hydrogen bonds between the carbonyl group of residue *i* and the amino group of residue $i + 4$ are shown as solid black lines. Coil peptide bonds (gray), peptide bonds with only carbonyl hydrogen bond (red), peptide bonds with only amino hydrogen bonds (blue), peptide bonds with both carbonyl and amino groups hydrogen bonded (purple), residues in helical conformation (green), residues in coil conformation (gray), and N and C caps (orange) are represented.

helix−coil relaxation kinetics is characterized by only two relevant kinetic phases. The fast (i.e., less than 20 ns) phase involves the reequilibration between α-helices of different lengths, and the slow (i.e., ∼200 ns) phase accounts for the equilibration between the coil and the ensemble of helices. However, all these experiments have been performed in model peptides with simple sequences that either are essentially homopolymers[18−20,22] or include just one single side chain−side chain interaction.[21] More recent *T*-jump experiments in a peptide of more complex sequence have revealed a surprisingly rich kinetic behavior.[1] Using specific ^{13}C labeling techniques, the authors observed that the apparent relaxation time of the nonexponential time course varied for peptides labeled in different regions. Furthermore, the observed relaxation time also depended on the magnitude of the *T*-jump to the same final temperature, becoming slower the larger the jump. These observations have been deemed incompatible with a nucleation−elongation description of the helix−coil kinetics. It was proposed instead that the rate of α-helix formation is determined by conformational search in the coil ensemble.[1] The explanation goes along the lines of previous explicit solvent molecular dynamics (MD) simulations of a penta-alanine peptide, which showed downhill helix nucleation with relaxation times of <1 ns.[23,24]

The higher resolution of these new laser *T*-jump experiments on ^{13}C labeled peptides provides stringent tests to kinetic theories of the helix−coil transition. Any valid theoretical description of α-helix formation should be able to reproduce the complex behavior observed in these experiments. In this regard, the "conformational search" interpretation is somewhat unsatisfactory because it only provides a qualitative picture and it does not explain the observation of different kinetics for different regions of the peptide. It also requires a coil ensemble that becomes increasingly more helix-like as temperature decreases and the absence of nucleation barriers. However, the analysis of previous equilibrium and laser *T*-jump data with models of the helix−coil transition indicates that the nucleation barrier is significant.[5,19,21,25] Molecular simulations predict smaller nucleation barriers,[23,26] perhaps because current molecular mechanics force fields have some bias toward the α-helix conformation. Another interesting theory describes the kinetics of α-helix formation by applying a mean first passage time approach to the original Zimm−Bragg equilibrium treatment.[27] The advantage of this approach is that it explicitly describes general statistical effects on the kinetics of α-helix formation, such as the interplay between many nucleation sites. Because it is based on a mean-field approach, this theory does not provide a microscopic description of helix−coil kinetics. So, the important question that arises is whether a detailed kinetic model of the helix−coil transition can reproduce the new *T*-jump results. Here we investigate this issue by formulating a more sophisticated version of the nucleation−elongation helix−coil theory previously used to interpret early *T*-jump experiments. In this new helix−coil kinetic model, we introduce the dependence on the amino acid sequence and the double-sequence approximation. To account for the sequence dependence of the helix−coil transition, we have directly used the set of parameters of the helix−coil equilibrium algorithm AGADIR.[28] The double-sequence approximation, that is, allowing two nonoverlapping helical segments to be simultaneously present in a single molecule, constitutes a critical improvement in reproducing the mechanism of helix formation. The double-sequence approximation allows helices to break from the middle and allows short helical segments to merge into longer helices. Finally, to directly compare the kinetic simulations and experimental data, we model the amide I band spectra of the peptide bond chromophores as Gaussian curves. We then calculate the time-dependent Fourier transformed infrared (FTIR) signal from the probability distribution as a function of time generated by the model. Our calculations show that the nucleation−elongation kinetic theory reproduces the complex kinetic behavior observed by laser *T*-jump infrared experiments in ^{13}C labeled peptides. Furthermore, the analysis of our simulations reveals the physical origin of the nonexponential time-courses and the mechanistic underpinnings behind the observation of different relaxation times for various regions of the peptide and for perturbations of increasing magnitude.

The Model

Equilibrium. In our model, the basic conformational unit is the peptide bond. Each peptide bond can be in two different states: helix and coil. The peptide bond is in the helix conformation if the dihedral angles ψ_i (with residue before the peptide bond) and ϕ_{i+1} (with residue after the peptide bond) are simultaneously in α-helical values. All other combinations of dihedral angles are included in the coil state, which is used as the reference state (statistical weight $rc = 1$). Because fixing the pair of dihedral angles in helical values involves decreasing the entropy of the peptide bond, the intrinsic statistical weight of the helix state ($h_{in} = \exp(\Delta S^{H-RC}/R)$) is <1. The specific values of h_{in} depend on the chemical nature of the two flanking residues (see below). Fixing several peptide bonds in a row in the helical state becomes progressively more unfavorable, giving rise to the characteristic nucleation of the helix−coil transition (e.g., statistical weight $(h_{in})^n$ for *n* residues). However, at a given length the stretch of α-helix is long enough to allow for the formation of stabilizing backbone interactions. These interactions are hydrogen bonds between the CO group of residues at *i* position and the NH group of residues at position $i + 4$ (see Figure 1), dipole−dipole, and van der Waals.[25,29] The net

balanceof the backbone interactions is favorable. Therefore, the statistical weight of adding a new peptide bond to a prenucleated helix stretch is the product of the intrinsic helical weight (h_{in}) and the weight from all backbone interactions ($h_{bb} = \exp(-\Delta G_{bb}/(RT))$). This is the process referred as elongation in classical helix−coil theory. For some sequences (e.g., polyalanine), the elongation statistical weight ($h_{in}h_{bb}$) is >1, resulting in an intrinsic propensity to form α-helices that grows with the length of the α-helix. In addition to the aforementioned factors, the stability of α-helical conformations is affected by sequence-dependent interactions. Such interactions are primarily i, $i + 3$ and i, $i + 4$ side chain−side chain interactions, interactions of charged residues with the α-helix macrodipole, and the N and C capping effects. To parametrize all the contributions to α-helix stability, we use the set of parameters of the helix−coil algorithm AGADIR.[28] In the context of AGADIR, h_{bb} corresponds to the mean residue enthalpic contribution, and it appears after fixing four residues in helical conformation plus the N and C caps.[25] Mapping the residue description of AGADIR into our peptide bond based model (see Figure 1) implies defining a segment of five consecutive peptide bonds in helical conformation as the helix nucleus. Addition of each additional peptide bond to the helix involves the net stabilization of the helix by one mean residue enthalpic contribution (h_{bb}). The intrinsic helix statistical weight (h_{in}) for each peptide bond in the helix segment is derived from the AGADIR intrinsic propensity parameter for the 20 amino acids[28] using the simple expression $h_{in} = \exp(-(\Delta G_{intri,i} + \Delta G_{intri,i+1})/(2RT))$. The N and C cap weights are taken directly from AGADIR[25] and are assumed to arise from the residue right before the first helical peptide bond for the N cap (n) and the residue right after the last helical peptide bond for the C cap (c). The parameters for all other sequence-dependent interactions are taken directly from AGADIR[28] and used to calculate the total statistical weight of each helical segment as the product of all the relevant weights. In AGADIR, segments of α-helix shorter than the nucleus of four residues plus the caps are not explicitly included because they are very low probability species.[25,28] In our model, we seek a detailed kinetic description of the process of α-helix formation, so we include these short helical segments. To calculate the statistical weight of helices of one to four helical peptide bonds in the simplest possible way, we assume that the only energetic factors that are relevant for short segments of helix are the intrinsic helix statistical weights and the caps. Thus, the statistical weight of a segment of j helical peptide bonds, j being <5, is simply expressed as $n(h_{in})^j c$.

With two states for each peptide bond, the model produces 2^n conformations for a peptide of n peptide bonds ($n = 20$ in the peptides analyzed in this work resulting in $2^{20} = 1\,048\,576$ species). However, the cost of helix nucleation makes it very improbable to find more than one α-helix segment in a short peptide. It is for this reason that the so-called single-sequence approximation—i.e., assuming that only one helical segment can be present at any given time in each molecule—has been found to reproduce the equilibrium behavior of peptides of less than 50 residues with great accuracy.[5,7,25] The single-sequence approximation, however, imposes severe constraints in the way α-helices form and break away because it only allows growth and melting from the ends. To include the merging of helical segments and the breaking from any position of the helix, we use here the double-sequence approximation. For a peptide of 20 peptide bonds, the number of possible conformations reduces from 1 048 576 to the 6196 conformations with 1, 2, or no helical segments. The partition function in the double-sequence approximation is expressed as

$$Q = 1 + \left(\sum_{i=1}^{n}\sum_{j=1}^{n-i+1} w_{ij}\left(1 + \sum_{p=1}^{n-i-j}\sum_{q=i+j+1}^{n-p+1} w_{pq}\right)\right)$$

where $w_{ij} = \exp(-\Delta G_{ij}/(RT))$ and $w_{pq} = \exp(-\Delta G_{pq}/(RT))$ are the statistical weights of helical segments of i and p number of peptide bonds that start at positions j and q of the molecule, respectively. The statistical weights of such helical segments are calculated as described above, and the statistical weight of residues in the coil state (rc) is 1 by definition. The probability for any given conformation is simply obtained as $w_{ji}w_{pq}/Q$, in which w_{ji} and w_{pq} are set to 1 for $i = 0$ and $p = 0$, respectively. The changes in the distribution of probabilities as a function of temperature are calculated as in AGADIR.[31]

Kinetics. The elementary kinetic steps in the model are the rotation of single peptide bonds from coil to helix (on rate) or from helix to coil (off rate). To construct the on and off rates, we assume an elementary transition state in which the peptide bond is already restricted in helical angles but is not able to form any interactions.[21,32] The on rate for a given peptide bond is expressed as $k_{on} = k_o h_{in}$, where k_o is a preexponential factor that defines the elementary rotation rate of peptide bonds. k_o is an adjustable parameter in the model and sets the absolute time scale for the different processes associated with helix formation. The temperature dependence of k_o is assumed to be inversely proportional to the change in water viscosity with temperature. In all of the calculations described in this work, we use $k_o = 2.5 \times 10^8\ s^{-1}$ at 1 cP. The off rate for the peptide bond is defined by detailed balance as $k_{off} = k_o h_{in} w_{final}/w_{initial}$, where w_{final} and $w_{initial}$ are the statistical weights of the final and initial conformation, respectively. The master equation is defined by these on and off rates and the kinetic rule that each conformation is connected to any other conformations accessible by rotation of single peptide bonds. For a peptide of n peptide bonds in the double-sequence approximation, this implies that the full coil and all conformations with a single helical segment are connected to n other conformations because rotations of each of the n peptide bonds are possible. Conformations with two helical segments are only connected to conformations in which one of the two helical segments is one residue longer or shorter. For conformations with no end effects (i.e., two helical segments that are more than one peptide bond apart and do not reach the N or the C terminus of the peptide), this typically means eight kinetic connections. Therefore, two helical segments in the same molecule can increase and decrease in length and can merge into one longer helix, but they cannot break into a larger number of shorter helices. This inherent limitation of the kinetics in the double-sequence approximation does not have a significant effect on the mechanistic picture of α-helix formation. The reason is that in short peptides conformations with more than two helical segments are expected to be very transient. Extensive stochastic kinetic simulations with the complete 2^n species helix−coil model show, indeed, that for 20-residue peptides cohabitation of more than two helical segments in a single molecule has a half-life of <400 ps. The vast majority of such transitions correspond to rapid flip-flops of single peptide bonds (data not shown). To simulate the relaxation kinetics induced by laser-induced temperature jumps, we integrate the master equation at the final temperatures using as initial conditions the distribution of probabilities calculated at the temperatures before the T-jumps are exerted. The master equation is expressed in matrix form and solved numerically using standard matrix methods for stiff problems to integrate the resulting sparse rate matrix.[32]

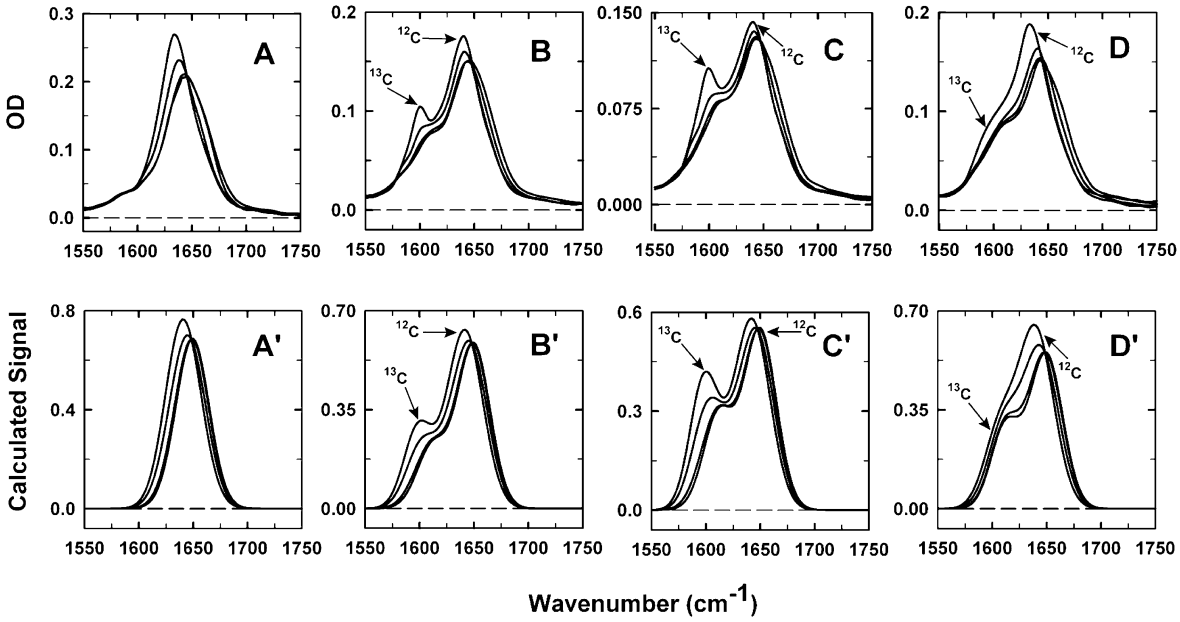

Figure 2. Amide I band infrared spectra as a function of temperature. The upper panels show the experimental amide I spectra at different temperatures (276, 303, 330, and 348 K) obtained by Huang et al.[1] The lower panels show the theoretical amide I spectra calculated at the same temperatures. In each panel the spectrum with highest peak intensity corresponds to the lowest temperature. As temperature increases the spectra broaden and the intensity of the peak decreases.

Results and Discussion

The peptides previously analyzed by the laser *T*-jump technique have the general sequence Ac-YGSPEA$_3$KA$_4$KA$_4$r-CONH$_2$, in which the carbonyls of each of the three groups of alanines are alternatively labeled with ^{13}C. This sequence has been designed to have marginal stability at low temperatures.[33] In agreement with this assertion, the original AGADIR algorithm predicts a helical content of ∼60% at 273 K for the 20 peptide bond peptide (19 residues, acetylated at the N-terminus and amidated at the C-terminus) in which the nonnatural C-cap D-arginine[34] was substituted by the best natural C-cap available (i.e., glycine). However, it is difficult to obtain a precise experimental estimate of the helical content to compare with the calculations, because no far-UV circular dichroism (CD) experiments have been reported for this series of peptides. CD data on a somewhat related peptide in which the SPE motif is substituted with GKA is in agreement with the prediction by AGADIR. In our model, we use parameters of AGADIR with glycine substituting for D-arginine. But, because we explicitly include conformations with one to four peptide bonds that are ignored in AGADIR,[25] we need to recalibrate the basic helix stabilization parameter. Conformations with only one to four peptide bonds in helix do not make hydrogen bonds and, for all practical purposes, belong to the coil ensemble. Including these conformations results in a large, entropically driven, increase in the stability of the coil ensemble. To compensate for this entropic effect, we have increased the strength of the mean residue enthalpic contribution to a value of −1.04 kcal/mol per peptide bond elongating the helix (see below).

The equilibrium behavior of the Ac-YGSPEA$_3$KA$_4$KA$_4$r-CONH$_2$ sequence has been analyzed experimentally using Fourier transformed infrared spectroscopy (FTIR), which provides the reference for infrared laser *T*-jump experiments.[1,33] The FTIR analysis of variants of the peptide ^{13}C labeled in specific sets of carbonyls allows monitoring of the thermal melting of different regions of the molecule. The amide I spectra obtained by Huang et al.[1] in the unlabeled peptide and in peptides labeled at the N-terminus (labels in positions 6−8), middle (labels in positions 10−13) and C-terminus (labels in positions 15−18) are shown in Figure 2 (panels A−D) for reference. Difference spectra obtained by subtracting the spectrum at the lowest temperature are shown in Figure 3 (panels A−D). The data on the unlabeled peptide (panel A of Figures 2 and 3) show that helix melting is characterized by a shift in the amide I band from ∼1635 to ∼1650 cm^{-1}. ^{13}C labeling decreases the amide I frequency by ∼40 wavenumbers, making it possible to monitor the unfolding of the labeled and unlabeled regions of the peptide independently. This is clearly observed in the experimental amide I infrared spectra of the three ^{13}C labeled peptides (Figure 2, panels B−D), and in their difference spectra (Figure 3, panels B−D). Interestingly, the melting behavior is quite different for each of the labeled peptides. Labeling the middle alanines results in a ^{13}C helix peak (∼1600 cm^{-1}) of very high intensity, while labeling at the C-terminus produces a broad and low intensity ^{13}C helix shoulder. The ^{13}C helix peak is clearly observable in the N-terminal labeled peptide, but it is less intense than that in the middle labeled peptide. These results provide a means to estimate the helical content of the peptide as a function of temperature from the derivative of the difference spectra. Furthermore, they give additional information about the distribution of α-helix content along the sequence as a function of temperature.

To directly compare the calculations from the helix−coil model with the experimental results, we calculate the amide I spectrum of the peptide as arising from the weighted average of the amide I band spectra of all the peptide bonds in the molecule. Here we represent the amide I band spectra of peptide bond chromophores as simple Gaussian curves. We have also used a Lorentzian representation with quite similar results. Normal-mode analysis indicates that the amide I transition is primarily due to the stretching of the C═O bond with a smaller but still significant (i.e., ∼25%) contribution from the stretching of the N−H bond.[35,36] Therefore we classify peptide bonds in different spectral groups on the basis of their hydrogen bonding status. The amide I frequencies for the different spectral groups are chosen on the basis of the typical values described for

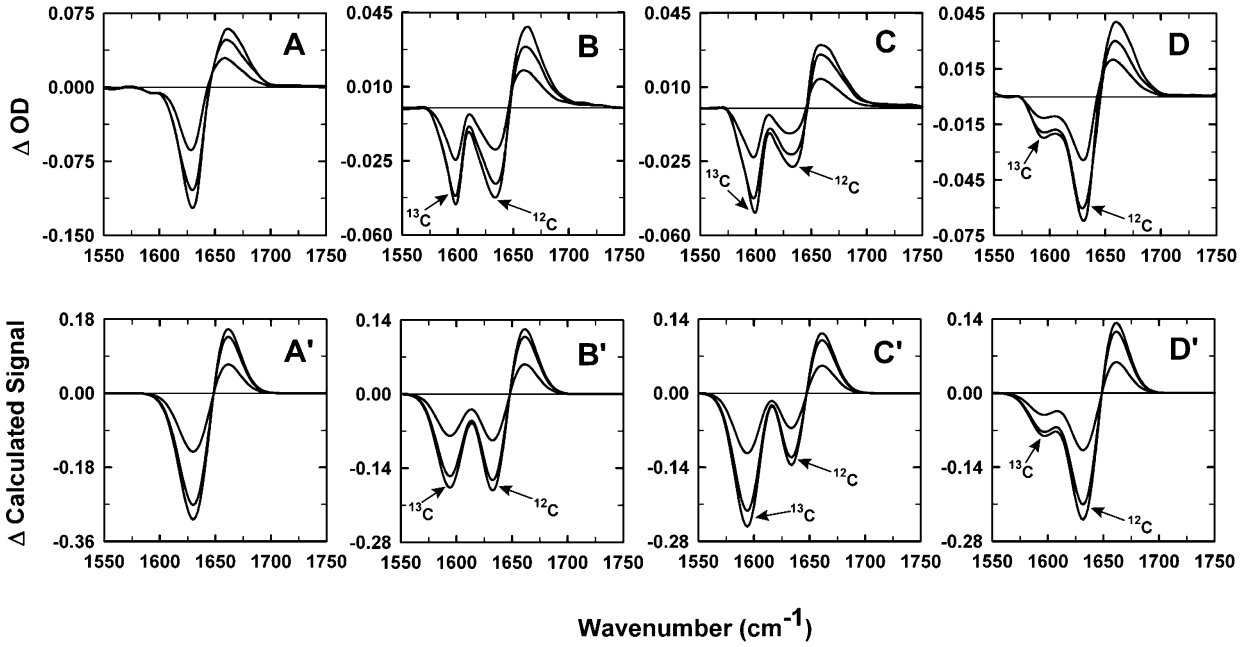

Figure 3. Difference amide I band spectra. Difference spectra are calculated by subtracting the spectrum at 273 K. The upper panels show the experimental difference spectra obtained by Huang et al.[1] Theoretical difference spectra are shown in the lower panels. In all cases, the curves correspond to spectra at 303, 330, and 348 K in order of increasing intensity.

TABLE 1: Spectral Parameters Used in Modeling Amide I Band Spectra[a]

	peptide bonds	mean μ (cm^{-1})	standard deviation, σ (cm^{-1})	relative intensity
nonlabeled (^{12}C)	HB C═O	1639	15	1.2
	HB NH	1646	15	1.2
	HB C═O and NH	1636	15	1.0
	helical NHB	1650	15	1.3
	coil	1650	15	1.3
labeled (^{13}C)	HB C═O	1601	13	1.8 × 1.2
	HB NH	1608	13	1.8 × 1.2
	HB C═O and NH	1598	13	1.8
	helical NHB	1612	13	1.8 × 1.3
	coil	1612	13	1.8 × 1.3

[a] HB C═O = helical peptide bonds with only C═O hydrogen-bonded; HB NH = helical peptide bonds with only NH hydrogen-bonded; HB C═O and NH = helical peptide bonds with both C═O and NH hydrogen-bonded; helical NHB = helical peptide bonds with no hydrogen bonds; coil = peptide bonds in coil conformation.

deuterated α-helix and coil spectra.[36] Non-hydrogen-bonded peptide bonds (shown in gray color in the example of Figure 1) are modeled as a Gaussian curve with a maximum at 1650 cm^{-1}. This group includes coil peptide bonds and helical peptide bonds in helical segments that are too short to make hydrogen bonds. Peptide bonds in which both the carbonyl and the amino groups are hydrogen-bonded (purple in Figure 1) are modeled with a Gaussian curve with the maximum shifted to 1636 cm^{-1}. Peptide bonds with only the carbonyl hydrogen-bonded (red in the example of Figure 1) are represented as Gaussian curves with a maximum at 1639 cm^{-1}. Peptide bonds in which only the amino group is hydrogen-bonded (blue in example of Figure 1) are represented as Gaussian curves with maximum at 1646 cm^{-1}. The effect of the isotopic ^{13}C labeling on the amide I spectrum is modeled as a shift of 38 wavenumbers and an increase in transition dipole strength of the same magnitude for all spectral groups. The specific parameters for all of the spectral groups considered here are shown in Table 1. The theoretical amide I spectra for the four different peptides, calculated using such a simple description of the basis amide I spectra and the probabilities as a function of temperature for the 6196 species of the double-sequence approximation model, are shown in Figure 2 (panels A′-D′). In these calculations, glycine is used in place of D-arginine, and the intrinsic propensity of proline in the first positions of the helix is considered equal to that of a glycine, because in those positions the presence of the proline imino group does not hinder formation of hydrogen bonds.[37]

The theoretical amide I spectra calculated with such a procedure and a value of −1.04 kcal/mol for the mean enthalpic contribution are shown in Figure 2 (panels A′−D′). Difference spectra with reference to the lowest temperature are shown in Figure 3 (panels A′−D′). The theoretical spectra reproduce the general features observed experimentally, although the shape of the experimental spectra is obviously non-Gaussian. The success of the calculation is better appreciated in the difference spectra (Figure 3), which show that the Gaussian representation reproduces the relative changes quite precisely. These include the ratio between minima and maximum, the changes in intensity as a function of temperature, and the relative intensity of the labeled and unlabeled peaks. While similar calculations using Lorentzian curves result in theoretical spectra that are more similar to the experimental ones, the difference spectra are less faithfully represented due to the characteristic wings of the Lorentzian function. It is apparent from the comparison between experimental and theoretical difference spectra (Figure 3) that a value of −1.04 kcal/mol for the mean enthalpic contribution exactly compensates for the entropic stabilization of the coil ensemble. The equilibrium melting transition obtained from this calculation displays a T_m of ∼293 K and is shown in Figure 4. Figures 2 and 3 also show that the theoretical spectra reproduce the spectral changes induced by placing the ^{13}C labels in different regions of the peptide. As in the experiment, the theoretical ^{13}C band has the strongest relative intensity when the labels are placed in the middle, and the weakest when they are placed at the C-terminus. This is the case even considering that the N-terminally labeled peptide only has three labeled carbonyls compared to the four carbonyls that are labeled at the C-terminus. Similar results were obtained with other combinations of spectral parameters (data not shown), indicating

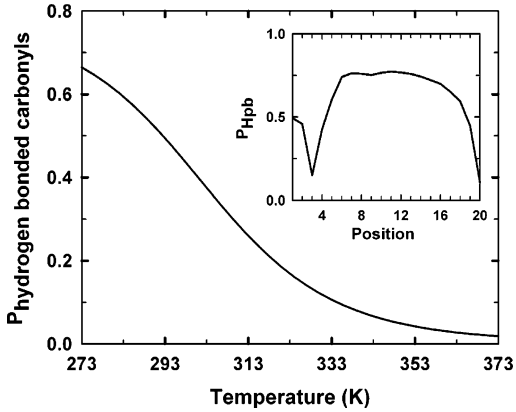

Figure 4. Theoretical equilibrium thermal denaturation. The figure shows the probability of hydrogen-bonded carbonyls as a function of temperature. The inset shows the probability of finding each peptide bond in helical dihedral angles calculated at the T_m (293 K).

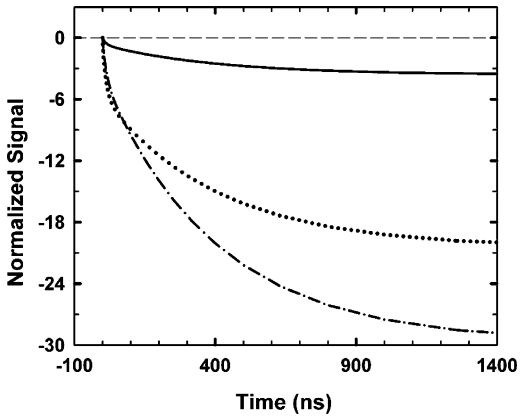

Figure 5. *T*-jump relaxation kinetics at different observation frequencies. Theoretical kinetic relaxations for the peptide labeled in the middle region are shown as a dashed−dotted line (observation frequency 1600 cm^{-1}) and a dotted line (observation frequency 1635 cm^{-1}). The theoretical kinetic relaxation expected for an unlabeled peptide upon excitation at 1600 cm^{-1} is shown as a solid line. In all cases, the signal has been normalized to 0 at $t = 0$.

that this general observation does not depend on the specific modeling of the basis spectra. The analysis of the results produced by the model indicates that the relative intensity of the labeled peak reflects the helix fraying at the ends that is so characteristic of the helix−coil transition.[4] The helical content is indeed highest at the center of the molecule, decreasing at the ends (inset to Figure 4). The model reveals that the helical content is minimal at the third peptide bond because the serine followed by the proline act as a strong helix stop signal. The population at the very N-terminal end is due mainly to very short non-hydrogen-bonded helical segments (i.e., one or two peptide bonds) that do not bypass the serine residue. After the third peptide bond, the helix population increases steadily reaching a maximum value already at the sixth peptide bond. The C-terminal region shows fraying that is partially damped by the C-capping effect. In addition to a high degree of fraying, the intensity of the ^{13}C peak in the peptide labeled at the C-terminus is further lowered by the fact that only two out of the four labeled C-terminal carbonyls is susceptible to making a hydrogen bond.

Kinetic models of the helix−coil transition predict that in homopolymers the relaxation to equilibrium after a perturbation should involve two distinct kinetic phases.[19] The fast phase corresponds to reequilibration between helices of different lengths and, therefore, is controlled by series of (de)propagation steps. The slow phase accounts for global reequilibration involving the crossing of the nucleation barrier. In contrast to previous laser *T*-jump studies,[18−22] the experiments of Huang et al. in the Ac-YGSPEA_3KA_4KA_4r-$CONH_2$ sequence reveal nonexponential time courses for kinetic relaxations following nanosecond *T*-jumps. The time-courses can be fitted to either a sum of two exponential functions,[38] or a stretched exponential with $\beta > 0.7$,[1] in addition to an "instantaneous" (<10 ns) component that is convoluted with the response of their instrument.[1,38] The "instantaneous" component must include some fractional amplitude of the faster regime and, possibly, intrinsic changes in the amide I spectrum induced by increasing temperature. Furthermore, Huang et al. find that the relaxation kinetics of the peptide labeled in the middle look apparently different depending on the observation frequency.[33] Kinetic simulations of the Huang et al. *T*-jump experiment with our helix−coil model in which the amide I spectra are assumed to be temperature-independent reproduce these observations quite well (Figure 5). From the simulations, we can conclude that the differences in the relaxation kinetics when observed at 1600 cm^{-1} (i.e., labeled peak) or at 1630 cm^{-1} (i.e., unlabeled peak) result mainly from changes in the relative amplitudes of the fast and slow kinetic phases. This effect would be further enhanced if the amide I spectra happen to have a strong dependence with temperature. The simulations with the helix−coil model also give a simple explanation for the observation of nonexponential *T*-jump kinetics in this sequence. All previous helix−coil *T*-jump experiments have been carried out in peptides that are essentially made of alanine, lysine, and arginine. The intrinsic propensity of these three amino acids is very high.[5] High intrinsic helical propensity results in fast propagation rates and, accordingly, in a fast-phase relaxation that is too fast to be resolved with current implementations of the laser *T*-jump technique. The Huang et al. sequence has a segment at the N-terminus with very low intrinsic propensity, so that helix stabilization relies much more heavily on additional factors such as N- and C-capping effects. Strong capping makes the helix−coil transition more cooperative, the propagation rates more heterogeneous, and the fast phase sufficiently slow as to be detected in experiments with 10 ns time resolution.

The heterogeneity in propagation rates and preferential stabilization of long helical segments through capping can have strong effects on the relaxation kinetics of this sequence versus the kinetics expected for simpler polyalanine sequences. Especially, since the slow propagation rates are not distributed uniformly through the molecule but are clustered at the N-terminus. In principle, these subtle effects can be investigated experimentally by monitoring the relaxation kinetics in different regions of the peptide. Huang et al. have performed such experiments by measuring local relaxation kinetics after *T*-jump perturbations. When monitoring the relaxation kinetics of the ^{13}C labeled peak by exciting at 1600 cm^{-1}, Huang et al. found that labels placed at the N-terminus or in the middle of the peptide had very similar relaxation kinetics after normalizing for differences in signal. However, the relaxation kinetics of the C-terminally labeled peptide seemed much faster (inset to Figure 6A). In Figure 6, we show kinetic simulations of these experiments, in which a temperature jump of 10 K to a final temperature of 288 K is applied to each of the three labeled peptides. The calculated 1600 cm^{-1} signal as a function of time is shown normalized for comparison with experiment. The theoretical time courses are in close agreement with the kinetics observed experimentally. The relaxation of the N-terminal and middle peptides are indistinguishable, while the normalized

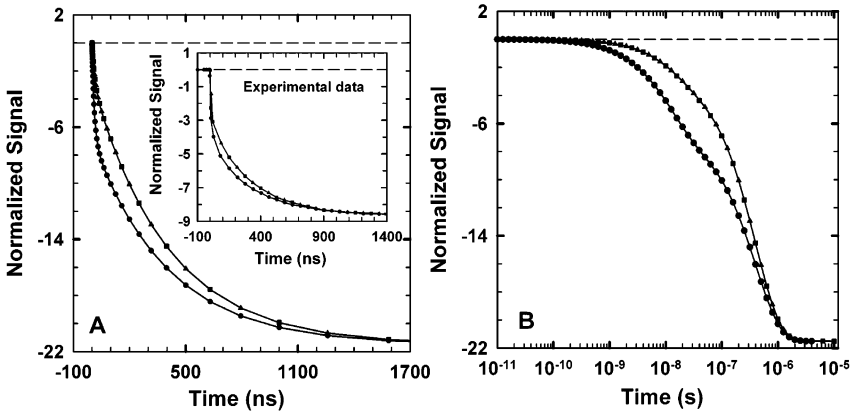

Figure 6. Relaxation kinetics probing different regions of the peptide. Panel A shows the theoretical relaxation kinetics at 1600 cm^{-1} of peptides labeled at the N-terminus (▲), middle region (■), and C-terminus (●). Following Huang et al.,[1] all the time courses have been normalized to 0 at $t = 0$ and to the signal of the N-terminally labeled peptide at 10 μs. The scaling factors are 0.72 for the middle labeled and 1.6 for the C-terminally labeled peptides. The inset shows the original experimental data of Huang et al.[1] Panel B shows the same relaxation kinetics as shown in panel A but plotted on a logarithmic time scale. In both panels A and B, the calculated change in signal has been scaled by 10^3.

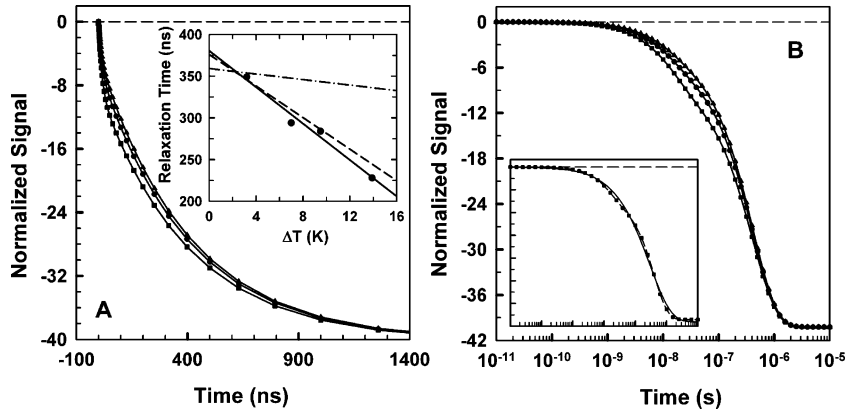

Figure 7. Relaxation kinetics of peptides labeled in the middle region after *T*-jumps of different size. Panel A shows the theoretical relaxation kinetics at a final temperature of 288 K after a *T*-jump of 3 (▲), 15 (●), and 40 K (■). Following Huang et al.,[1] all the time courses have been normalized to 0 at $t = 0$ and to the signal after the 15 K jump at 10 μs. The scaling factors are 0.62 for 3 K and 3.96 for 40 K jumps. The inset shows the dependence of the apparent relaxation time on the magnitude of the *T*-jump. The experimental results of Huang et al.[1] are shown as filled circles with a linear fit through the data (solid line). The dashed−dotted line shows the apparent relaxation time dependence on the *T*-jump size obtained in calculations using −1.04 kcal/mol for the mean enthalpic contribution. The dashed line shows the apparent relaxation time dependence on the *T*-jump size obtained in calculations using −1.18 kcal/mol for the mean enthalpic contribution. Panel B shows the same relaxation kinetics as shown in panel A but plotted on a logarithmic time scale. The inset shows the relaxation kinetics after a *T*-jump of 40 K (■) and fits to a double-exponential function (dashed line) and to a stretched exponential function with $\beta = 0.64$ (solid line). In both panels A and B, the calculated change in signal has been scaled by 10^3.

C-terminal relaxation appears faster. When the time courses are plotted in a logarithmic time scale (Figure 6B), it becomes evident that the source for the apparently faster relaxation kinetics of the C-terminal region is the fast phase, which has a larger relative amplitude (increasing from ∼15% to ∼30%) and shorter relaxation time.

The previous set of experiments and calculations is a clear example of how the relaxation kinetics that is observed for the helix−coil transition depends on the probe used to monitor the reaction. A complementary kinetic test of helix−coil theory is to investigate the effect of the magnitude of the initial perturbation in the relaxation kinetics. In fact, Huang et al. have reported that the relaxation rate in the middle labeled peptide seems to depend on the size of the *T*-jump.[1] To quantify this effect, Huang et al. fitted the experimental nonexponential relaxation kinetics to stretched exponential functions (the final β parameter randomly varying between 0.75 and 0.85 for different jump sizes) and plotted the obtained relaxation rate as a function of the magnitude of the temperature jump to the same final temperature of 288 K. This analysis indicated that the observed relaxation time depended linearly on the size of the *T*-jump with a slope of approximately −10 ns K^{-1} and intersect with the abscissa at ∼390 ns (see inset to Figure 7A). In these experiments, changes in the amplitude of the so-called "instantaneous" component were also reported.[1] To investigate whether our helix−coil model could reproduce these observations, we carried out kinetic simulations at 288 K starting with population distributions calculated at the initial temperatures of the experiment. The results are shown in Figure 7. It can be seen that in the simulations the apparent relaxation kinetics also depend on the size of the temperature jump, becoming apparently faster the larger the difference between initial and final temperatures (Figure 7A). Displaying the data in a logarithmic time scale reveals that the differences in relaxation kinetics arise again from changes in the relaxation time and relative amplitude of the fast phase. However, the effect is significantly weaker for the calculations. The calculated kinetics are clearly biphasic, but to reproduce the experimental analysis the time evolution can be fitted to stretched-exponential functions with β-values of ∼0.7 (see inset of Figure 7B). Fitting the theoretical curves to stretch exponentials renders a slope of just approximately −2 ns K^{-1}. What is the origin of this discrepancy? In the calculations, we observe that for much higher temperature jumps the apparent relaxation time continues to decrease linearly (e.g.,

see a jump of 40 K in Figure 7A). Therefore, one possible explanation is that the experimental perturbation is of higher magnitude than the theoretical perturbation. This could happen if the parameters of AGADIR underestimate the temperature dependence of the helix−coil transition for this peptide or if the size of the experimental *T*-jumps was underestimated by Huang et al. Alternatively, we have observed that the slope for the relaxation time increases sharply in conditions of higher helix stability. A mean residue enthalpic contribution of −1.18 kcal/mol increases the T_m from ∼293 (Figure 4) to ∼305 K, placing the final *T*-jump temperature (288 K) well below the midpoint. Kinetic simulations performed under these conditions result in a slope similar to that determined experimentally (inset of Figure 7A). Although such stability is incompatible with equilibrium and other kinetic data, the calculation highlights that to reproduce the experimentally measured slope the relative amplitude of the slow phase must be <40%. The reason is that the apparent relaxation time obtained by fitting to a stretched exponential function depends on which of the two phases predominates at the time at which the total signal becomes $S_{fin} - \Delta S/e$. This realization immediately suggests a more likely explanation for the discrepancy between the experimental and theoretical results. In the experiment, the fast phase is only partially resolved, and there is an additional "instantaneous" component, which probably reflects the temperature dependence of the amide I spectrum. Therefore, the "instantaneous" and fast phase amplitudes are mixed together decreasing the relative amplitude of the slow phase. This effect would produce an overestimation of the experimental slope because the "instantaneous" amplitude is expected to increase proportionally to the magnitude of the *T*-jump.

The experiments of Huang et al.[1,38] dramatically demonstrate the kinetic complexity of the process of α-helix formation. Here we have shown that all of their results are compatible with a simple nucleation−elongation model. The model indicates that such kinetic complexity arises from a combination of fundamental properties of the helix−coil transition and specific details of the amino acid sequence used in these investigations. This is a very important result that supports the general validity of nucleation−elongation as a mechanism of α-helix formation. Furthermore, having a quantitative microscopic model of the process gives the unique opportunity to delve into the physical origin of the observed kinetic complexity. Our results reveal that, despite the high level of kinetic detail in the model (i.e., 6196 coupled differential equations), it is possible to rationalize the most basic features of the helix formation process using a simple one-dimensional projection of the free energy as a function of the number of helical peptide bonds. Such a free energy profile has two broad minima separated by a shallow barrier arising from the cost of helix nucleation (Figure 8A). An increase in temperature produces two perturbations in the surface. The first one is a shift of the helical minimum to lower values, which results from the decrease in average helix length (see Figure 8B). The second effect is an overall destabilization of the helix basin of attraction, resulting in an increase of the coil population (Figure 8B). These general features are still present if the free energy surfaces are calculated with the complete model in which the peptide is allowed to have more than two simultaneous helical segments (inset to Figure 8A). The fast kinetic phase corresponds to the relaxation in the helical basin of attraction. It can be viewed as almost diffusive, and therefore, its relaxation time should be proportional to the displacement along the reaction coordinate (i.e., the decrease in average length). The slow phase accounts for the equilibration between the two minima. The slow phase is dominated by crossing the nucleation barrier. But, because the helix nucleation barrier is small, it also has a diffusive component. This makes the slow relaxation slightly sensitive to the changes in average helix length, as it has been argued before.[21] Interestingly, this description is quite similar to the "conformational diffusion" picture.[23] The main difference is that in this case diffusion is occurring in the helical region instead of in the coil region of phase space.

In the experiment in which ^{13}C labels are placed in different regions of the peptide (Figure 6), the free energy perturbation is the same for the three cases, but the decay of the signal depends quite drastically on where the labels are placed (Figure 8C). The 1600 cm^{-1} signal of the N-terminal and middle labels decays weakly as the average helix length decreases because all these labels are placed in the region of the molecule where there is less helix fraying (inset of Figure 4). The C-terminal labels are placed right at the end of the peptide, precisely in the region of largest helix fraying. Therefore, the signal decays much more abruptly (Figure 8C), making the C-terminal labels mostly sensitive to the shortening of very long helices. Accordingly, the C-terminal fast phase carries a large change in signal resulting in larger relative amplitudes and involves a greater extent of local motions. This effect can be easily assessed by plotting the temperature-induced changes in the distribution of probabilities weighted by the change in signal (Figure 8D). In this graph, the peak in the coil region with maximum at three peptide bonds is related to the size of the relative amplitude of the slow phase. The relative amplitude of the fast phase is related to the intensity of the positive shoulder at higher number of helical peptide bonds, and its relaxation time is proportional to the weighted displacement between the shoulder and the negative peak. The origin of shorter apparent relaxation times at lower initial temperatures is less intuitive. In that experiment (see Figure 7), the peptide is always probed in the middle region, and it is the *T*-jump size that changes (Figure 8E). In principle, it could be argued that the relaxation should become slower at lower initial temperatures, because the larger the temperature jump the more the displacement in the helical basin of attraction. However, at high stability, the average helix length approaches the maximum value and the population distribution becomes narrower. So, if the initial temperature is low, i.e., high helix stability, the redistribution of helices of different lengths is dominated by motion near the maximum number of helical peptide bonds. The average displacement is shorter and the relative amplitude of the fast phase increases, resulting in shorter apparent relaxation times. This complex effect becomes obvious when the redistribution of probabilities is shown weighted by the change in signal at 1600 cm^{-1} and normalized to the intensity of the random coil peak (Figure 8F).

Our theoretical analysis of the Huang et al. experiments reveals that the kinetic complexity they observe is inherent to the helix−coil transition. The complexity arises from the interplay between a small nucleation penalty and multistep propagation. It is also interesting to investigate whether the experiments provide additional information on the important issue of helix nucleation. We have approached this question by modifying the basic features of the model and comparing calculations carried out with the modified models and experiment. There are two basic ways of modifying the nucleation process: by changing either the size of the helix nucleus or the cooperativity of the helix−coil transition. The latter is easily achieved by changing the scale of the entropy cost involved in fixing peptide bonds in helical angles while keeping the same

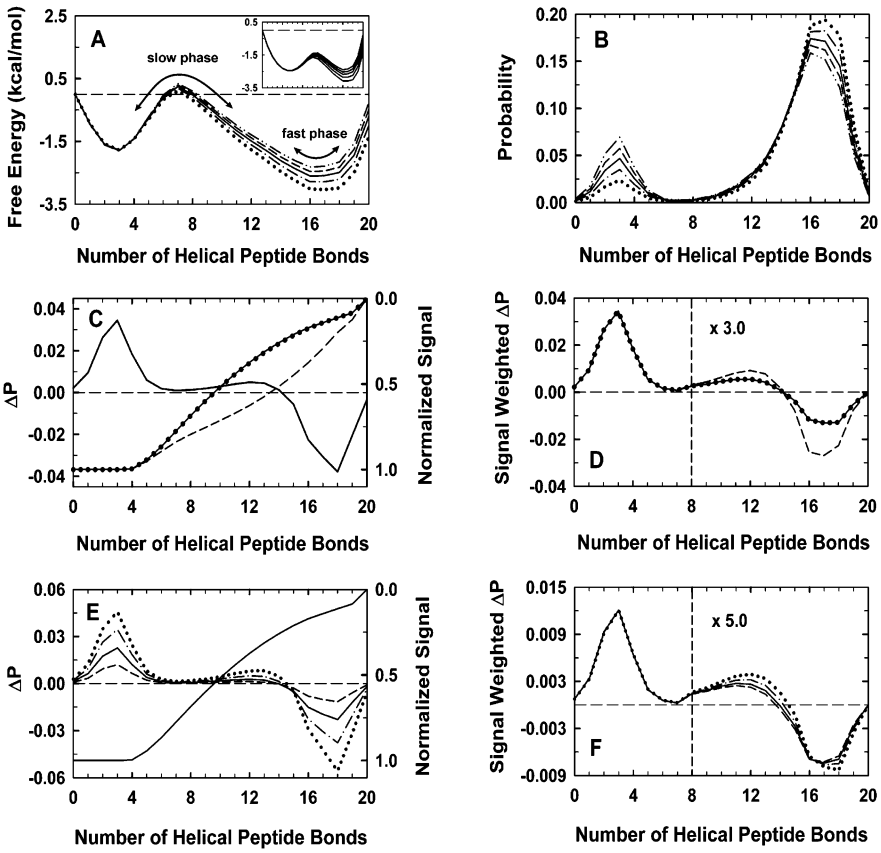

Figure 8. Understanding α-helix formation using 1-dimensional projections. Panel A shows a projection of the free energy of α-helix formation, i.e., as a function of the number of helical peptide bonds at 273 (···), 278 (− · −), 282 (—), 285 (− − −), and 288 K (− ··). The inset shows the same free energy surfaces (at temperatures decreasing from top to bottom) calculated with a complete partition function that includes all possible combinations of nonoverlapping helical segments. Panel B shows the distribution of probabilities at the same temperatures and using the same code for the lines. Panel C shows the redistribution of probabilities and change in signal for different probes after a temperature jump from 278 to 288 K: (left scale) $P_{288} - P_{278}$; (right scale) difference between the signal at 1600 cm^{-1} as a function of the number of helical peptide bonds and the signal at 1600 cm^{-1} of the full-length helix (20 helical peptide bonds); (—) difference in signal for N-terminally labeled peptide, (···) for middle labeled peptide, and (− − −) for C-terminus labeled peptide. Panel D shows the redistribution of probabilities as shown in panel C but weighted for the change in signal for each labeled peptide. The scale has been multiplied by a factor of 3 after seven peptide bonds to enhance visibility. Panel E shows the redistribution of probabilities and change in signal for the middle label after *T*-jumps of different size: (left scale, ···) $P_{288} - P_{273}$; (left scale, − · −) $P_{288} - P_{278}$; (left scale, —) $P_{288} - P_{282}$; (left scale, − − −) $P_{288} - P_{285}$; (right scale) change in signal as shown in panel C but just for the middle labeled peptide. Panel F shows the redistribution of probabilities as shown in panel E but weighted for the change in signal at 1600 cm^{-1} of the middle peptide. The code for the lines is as described for panel E. The scale has been multiplied by a factor of 5 after seven peptide bonds to enhance visibility.

T_m with opposing changes in the mean enthalpic contribution. We have tried many different combinations of these two parameters, and they all produce similar results in the kinetic tests outlined above, once the intrinsic rotation rate is readjusted to reproduce the experimental time scale. However, the conclusion is different for the size of the helix nucleus. The nucleus size determines the relative time scales of the fast and slow phases. This issue is of obvious importance and is still somewhat contentious since, on the basis of stopped-flow experiments on polyalanine peptides, it has been proposed that helix nucleation could take as long as milliseconds.[39] Moreover, the nucleus size is related to how the different energetic factors involved in helix formation balance each other out. Because the experiments by Huang et al. are the first ones in which both phases are simultaneously resolved, even if partially, they provide a quite useful benchmark to investigate the size of the nucleus. In calculations with different nucleus sizes, we have found that the original AGADIR nucleus (five peptide bonds) is close to the optimal. A nucleus of seven peptide bonds produced a slow phase that was ∼100 fold slower than the fast phase, while with a nucleus of three peptide bonds both phases tend to cluster together. Indeed, a nucleus of three produced results that looked already quite similar to those from calculations in which the helix was prenucleated to allow only for propagation. This result is very important because it settles the issue about the time scales for the different stages in helix formation. It also provides some support to the basic description of helix formation outlined in AGADIR.[25] In the same spirit of previous equilibrium studies of the helix−coil transition, the success of our simple nucleation−elongation kinetic model opens a new avenue of research on the kinetics of α-helix formation. Our model can be used to make specific predictions that can be tested experimentally, and experiment can be used to refine the parameters and theoretical description of the model.

Acknowledgment. We thank Eric R. Henry for providing the CVODE program package and for help in implementing our calculations in this program. We also thank Feng Gai for giving us permission to use his published data.[1] V.M. is a recipient of a Dreyfus New Faculty Award, a Packard Fellowship for Science and Engineering, and a Searle Scholar Award. This research has been supported in part by Grants 36601-AC4 from the Petrol Research Fund and R01-GM066800 from the National Institutes of Health.

References and Notes

(1) Huang, C. Y.; Getahun, Z.; Zhu, Y. J.; Klemke, J. W.; DeGrado, W. F.; Gai, F. *Proc. Natl. Acad. Sci. U.S.A.* **2002**, *99*, 2788−2793.
(2) Muñoz, V.; Serrano, L. *Nat. Struct. Biol.* **1994**, *1*, 399−409.
(3) Zimm, B. H.; Bragg, J. K. *J. Chem. Phys.* **1959**, *31*, 526−535.
(4) Lifson, S. *J. Chem. Phys.* **1961**, *34*, 1963.
(5) Chakrabartty, A.; Baldwin, R. L. *Adv. Protein Chem.* **1995**, *46*, 141−176.
(6) Marqusee, S.; Robbins, V. H.; Baldwin, R. L. *Proc. Natl. Acad. Sci. U.S.A.* **1989**, *86*, 5286−5290.
(7) Scholtz, J. M.; Hong, Q.; York, E. J.; Stewart, J. M.; Baldwin, R. L. *Biopolymers* **1991**, *31*, 1463−1470.
(8) Baldwin, R. L. *Biophys. Chem.* **1995**, *55*, 127−135.
(9) Rohl, C. A.; Scholtz, J. M.; York, E. J.; Stewart, J. M.; Baldwin, R. L. *Biochemistry* **1992**, *31*, 1263−1269.
(10) Rohl, C. A.; Baldwin, R. L. *Biochemistry* **1994**, *33*, 7760−7767.
(11) Bradley, E. K.; Thomason, J. F.; Cohen, F. E.; Kosen, P. A.; Kuntz, I. D. *J. Mol. Biol.* **1990**, *215*, 607−622.
(12) Liff, M. I.; Lyu, P. C.; Kallenbach, N. R. *J. Am. Chem. Soc.* **1991**, *113*, 1014−1019.
(13) Chakrabartty, A.; Schellman, J. A.; Baldwin, R. L. *Nature* **1991**, *351*, 586−588.
(14) Miick, S. M.; Todd, A. P.; Millhauser, G. L. *Biochemistry* **1991**, *30*, 9498−9503.
(15) Qian, H. *Biopolymers* **1993**, *33*, 1605−1616.
(16) Muñoz, V.; Serrano, L. *Curr. Opin. Biotechnol.* **1995**, *6*, 382−386.
(17) Gruenewald, B.; Nicola, C. U.; Lustig, A.; Schwarz, G.; Klump, H. *Biophys. Chem.* **1979**, *9*, 137−147.
(18) Williams, S.; Causgrove, T. P.; Gilmanshin, R.; Fang, K. S.; Callender, R. H.; Woodruff, W. H.; Dyer, R. B. *Biochemistry* **1996**, *35*, 691−697.
(19) Thompson, P. A.; Eaton, W. A.; Hofrichter, J. *Biochemistry* **1997**, *36*, 9200−9210.
(20) Lednev, I. K.; Karnoup, A. S.; Sparrow, M. C.; Asher, S. A. *J. Am. Chem. Soc.* **1999**, *121*, 8074−8086.
(21) Thompson, P. A.; Muñoz, V.; Jas, G. S.; Henry, E. R.; Eaton, W. A.; Hofrichter, J. *J. Phys. Chem. B* **2000**, *104*, 378−389.
(22) Lednev, I. K.; Karnoup, A. S.; Sparrow, M. C.; Asher, S. A. *J. Am. Chem. Soc.* **2001**, *123*, 2388−2392.
(23) Hummer, G.; Garcia, A. E.; Garde, S. *Phys. Rev. Lett.* **2000**, *85*, 2637−2640.
(24) Hummer, G.; Garcia, A. E.; Garde, S. *Proteins: Struct., Funct., Genet.* **2001**, *42*, 77−84.
(25) Muñoz, V.; Serrano, L. *Biopolymers* **1997**, *41*, 495−509.
(26) Daggett, V.; Levitt, M. *J. Mol. Biol.* **1992**, *223*, 1121−1138.
(27) Buchete, N. V.; Straub, J. E. *J. Phys. Chem. B* **2001**, *105*, 6684−6697.
(28) Muñoz, V.; Serrano, L. *J. Mol. Biol.* **1995**, *245*, 275−296.
(29) Yang, A. S.; Honig, B. *J. Mol. Biol.* **1995**, *252*, 351−365.
(30) Reference deleted in proof.
(31) Muñoz, V.; Serrano, L. *J. Mol. Biol.* **1995**, *245*, 297−308.
(32) Muñoz, V.; Henry, E. R.; Hofrichter, J.; Eaton, W. A. *Proc. Natl. Acad. Sci. U.S.A.* **1998**, *95*, 5872−5879.
(33) Huang, C. Y.; Getahun, Z.; Wang, T.; DeGrado, W. F.; Gai, F. *J. Am. Chem. Soc.* **2001**, *123*, 12111−12112.
(34) Schneider, J. P.; DeGrado, W. F. *J. Am. Chem. Soc.* **1998**, *120*, 2764−2767.
(35) Cheam, T. C.; Krimm, S. *J. Chem. Phys.* **1985**, *82*, 1631−1641.
(36) Krimm, S.; Bandekar, J. *Adv. Protein Chem.* **1986**, *38*, 181−364.
(37) Strehlow, K. G.; Robertson, A. D.; Baldwin, R. L. *Biochemistry* **1991**, *30*, 5810−5814.
(38) Huang, C. Y.; Klemke, J. W.; Getahun, Z.; DeGrado, W. F.; Gai, F. *J. Am. Chem. Soc.* **2001**, *123*, 9235−9238.
(39) Clarke, D. T.; Doig, A. J.; Stapley, B. J.; Jones, G. R. *Proc. Natl. Acad. Sci. U.S.A.* **1999**, *96*, 7232−7237.